REF: 4. Cashell, K.A., Elghazouli, AY. and Izzuddin, BA. (2011), Failure assessment of lightly reinforced floor slabs. II: Analytical studies, Journal of Structural Engineering 137(9): 989- 100.

Failure assessment of lightly reinforced floor slabs - Part 2: Analytical studies

Cashell K.A.[1], Elghazouli A.Y.[2] and Izzuddin B.A.[3]

Abstract

This paper describes numerical and analytical assessments focusing on the ultimate response of floor slabs. Simplified analytical models as well finite element simulations are described and validated against the experimental results presented in the companion paper. The simplified analytical model accounts for membrane action as well as the underlying mechanisms related to failure of floor slabs by either reinforcement rupture or compressive crushing of the concrete. In this respect, the significant influence of material properties including bond strength is considered in the model and described in detail. A detailed nonlinear finite element model is also employed to provide further verification of the simplified approach as well as to facilitate further understanding of the overall response. The results and observations of this study offer an insight into the key factors that govern the ultimate behavior. Finally, the models are applied under elevated temperature conditions in order to demonstrate their general applicability and reliability.

Keywords

Composite steel/concrete; composite slabs; lightly reinforced members; failure conditions; ductility; reinforcement fracture; nonlinear analysis.

1 Introduction

Recent years have seen significant advances to analytical procedures for assessing the performance of floor slab systems under fire conditions {Bailey and Moore, 2000; Elghazouli and Izzuddin, 2001; Izzuddin and Moore, 2002; Lim *et al*., 2002; Izzuddin *et al*., 2004; Elghazouli and Izzuddin, 2004; Omer *et al*., 2006; Clifton, 2006; Omer *et al*., 2010). This has been largely motivated by the necessity to develop more rational and cost-effective design procedures as well as a desire to attain a greater understanding of the fundamental behavioural mechanisms that occur in fire. There has been a move towards improving current codified methods, which are primarily of a prescriptive nature, by adopting more realistic design procedures based on structural performance. Before these can be developed and implemented, it is imperative that the response of floor slabs is fully assessed

[1] Senior Engineer, Steel Construction Institute, UK. (Corresponding author: k.a.cashell@gmail.com)
[2] Prof. of Structural Engineering, Dept of Civil & Environmental Eng, Imperial College London, UK, MASCE
[3] Prof. of Computational Structural Mechanics, Dept of Civil & Environmental Eng, Imperial College London, UK, MASCE

and understood, particularly at large deflections, using reliable and realistic modelling approaches coupled with the application of appropriate failure criteria. The ultimate behaviour however is relatively complex owing to the geometric and material nonlinearities involved as well as the large number of inter-related variables that influence the response.

In this context, several nonlinear analytical tools have been developed in recent years for the assessment of floor slab systems; these have generally provided realistic representations of the floor response (e.g. Bailey and Moore, 2000; Lim and Buchanan, 2002; Izzuddin *et al*., 2004; Izzuddin and Elghazouli, 2004; Omer *et al*., 2010). However, such detailed models, which typically utilize nonlinear finite elements, are often overly complex for direct application in design. Furthermore, they are generally based on assumptions which do not permit reliable assessment of the limiting ductility, or failure criteria. Prediction of the displacement and load levels corresponding to failure is as involved problem and necessitates a detailed treatment of the interaction between the concrete material and steel reinforcement, with due consideration of the appropriate loading and boundary conditions as well as the geometric and material nonlinearities.

In relation to the above discussion, simplified analytical models have recently been developed to predict the post-yield load-deflection response of floor slabs, as well as the level of deformation and load corresponding to failure, both at ambient and elevated temperature (Izzuddin and Elghazouli, 2004; Omer *et al*., 2006; Omer *et al*., 2010). The initial model (Omer *et al*., 2006) focussed on the failure state associated with rupture of the reinforcement. This is extended herein to account for the possibility of compressive failure around the slab edges. The developed models incorporate the effects of bond-slip, reinforcement stress-strain response, tensile membrane action and elevated temperature. Although this paper is concerned with the response of slabs without planar restraint, the model can be readily adjusted to satisfy various other boundary conditions. The simplified approaches are also complemented in this paper by more complex nonlinear numerical models in order to validate the assumptions made and to enable a more detailed assessment of the load-deflection response.

The companion paper (Cashell *et al*., 2011) presented the results and observations from an experimental investigation into the ambient response of floor slabs. The tests provided a fundamental insight into the ultimate performance of these members and the findings are employed in this paper to validate the proposed model. Towards this end, analytical predictions are compared with the results of the tests, with further verification provided through advanced nonlinear finite element simulations. The model is also employed to assess the elevated temperature effects with reference to available experimental results. Finally, a sensitivity study is conducted whereby the

influence of key considerations such as boundary conditions, bond strength and thermal effects are examined.

2 Finite element modelling

It has been shown that finite element modelling can provide valuable information regarding the behaviour of floor slabs under extreme loading conditions (Izzuddin *et al*., 2004; Clifton, 2006; Omer *et al*., 2010). The finite element simulations discussed in this paper were carried out using the nonlinear finite element program ADAPTIC (Izzuddin, 1994). The formulation of a new 2D shell element, denoted as *csl4*, has further advanced the capability of the program for analysing reinforced concrete and composite slabs (Izzuddin *et al*., 2004; Elghazouli and Izzuddin, 2004). The new shell element, as depicted in Fig. 1, combines computational efficiency with numerical accuracy and accounts for both geometric and material non-linearity, as well as the precise geometric orthotropy of the cross-section (Izzuddin *et al*., 2004). It was first developed as a means of overcoming the deficiencies of other more commonly-used elements such as the considerable dimensional simplifications inherent to 1D grillage elements, the geometric simplifications of using uniform-thickness 2D shell elements as well as the prohibitive computational expense of employing 3D solid elements. The *csl4* element accounts for: (i) the effect of the ribs on the membrane and bending actions transverse to the rib orientation; (ii) the influence of geometric nonlinearity due to large displacements and rotations; and (iii) the response of concrete under a non-monotonic strain variation and at elevated temperature. The element has also been shown to represent effectively the behaviour of composite floor slabs under extreme conditions, including those due to fire, blast, and earthquake loading.

With reference to material modelling, the steel reinforcement is characterised using a bilinear elasto-plastic model with kinematic strain hardening (*stl1*). On other hand, a robust uniaxial concrete model (*con11*) is utilised which accounts for compressive nonlinearity as well as tensile cracking (Izzuddin *et al*., 2004) For modelling unrestrained slabs, such as those discussed in the companion paper, vertical support is provided around all edges, as well as minimal planar restraint against rigid body movement.

Despite the advantages of the shell element adopted in the analysis, it is important to note that it is based on the smeared-crack approach and does not account for the bond-slip relationship between the reinforcement and the surrounding concrete. Therefore, the distribution of stress in the reinforcement would be sensitive to mesh density, resulting in unrealistic stress concentrations. Consequently, whilst these models should be able to represent the response history, they are inherently inadequate for the prediction of failure by reinforcement fracture. It is the primary

motivation behind the development of simplified analytical approaches such as that discussed in the following section.

3 Simplified analytical model

The one-dimensional strip model described in previous studies (Izzuddin and Elghazouli, 2004) has been used a basis to develop simple, yet realistic, mechanical models that account for failure of reinforced concrete slabs at ambient and elevated temperature (Omer *et al*., 2006; Omer *et al*., 2010). Both unrestrained and restrained members have been considered although emphasis is given herein to the response of unrestrained slabs, as described in the experimental study discussed in the companion paper (Cashell *et al*., 2011). For brevity, the initial version of the model is only outlined in this paper, whilst a full account, including various provisions for specific conditions, can be found elsewhere (Omer *et al*., 2006; Omer *et al*., 2010). Greater emphasis is given herein to the failure criteria adopted as well as the modifications and advancements that are proposed to the model.

The initial slab model (Omer *et al*., 2006) employs a kinematic approach to represent the overall plastic load-deflection response for unrestrained slabs, including the point at which failure occurs. The focus is on lightly reinforced slabs and hence it is assumed that failure is governed by fracture of the reinforcement across a full-depth crack. The model accounts for the important influence of bond between the steel reinforcement and concrete, the planar movement of the slab along the supports and the strain concentration in the steel reinforcement across the cracks. Additionally, it postulates that the segments of the slabs bounded by the yield lines rotate around the cracks in an almost rigid manner. It is assumed that the slab comprises a series of strip elements through the length and width of the element. The overall response is obtained by integrating the response of each strip (Fig. 2). As evident in the figure, a quarter of the slab is considered owing to symmetry.

The steel reinforcement is assumed to have a rigid-hardening constitutive relationship as shown in Fig. 3, where f_{sy} and f_{su} are the yield and ultimate strengths respectively; ε_{su} represents the ultimate strain and E_2 is the hardening modulus. On the other hand, the concrete is rigid in compression and does not contribute to the behaviour in tension. Furthermore, the bond-slip relationship is represented as a rigid-plastic idealisation which was previously validated (Cashell, 2009; Cashell *et al*., 2010) and is expressed as the total bond force per unit length per unit width (τ_b).

It was shown during the experimental programme described in the companion paper (Cashell *et al*., 2011) that failure of reinforced concrete floor slabs is usually governed either by reinforcement rupture across the full-depth failure crack, or crushing of the concrete in the proximity of the

supports. The former is more likely to occur in lightly reinforced members, or slabs with low-ductility reinforcement. In this case, failure occurs when the stress in the reinforcement across the failure crack reaches the ultimate capacity of the steel. The bond-slip length, x_d, is assumed to be bounded by half the distance between the crack and the intersection of the yield lines:

$$x_d = \frac{1}{2}\left(\frac{L_1}{2} - \eta L_1\right) \tag{1}$$

where L_1 is the longer span and η is the yield line geometric parameter, determined as a function of L_1 and the shorter span L_2, and given by:

$$\eta = \frac{1}{2\left(\frac{L_1}{L_2}\right)^2}\left(\sqrt{3\left(\frac{L_1}{L_2}\right)^2 + 1} - 1\right) \tag{2}$$

Thus, the predicted failure displacement ($U_{f,pred}$) is obtained from either Eq. (3a or b) according to:

$$U_{f,pred} = \sqrt{\frac{L_1}{2A_s E_2 \tau_b}}\left(T_u - T_y\right) \qquad if \;\; x_d \geq \frac{T_u - T_y}{\tau_b} \tag{3a}$$

$$U_{f,pred} = \sqrt{\frac{L_1}{2A_s E_2 \tau_b}\left(\left(T_u T_y + \tau_b x_d\right)^2 - 2\tau_b{}^2 x_d{}^2\right)} \qquad if \;\; x_d < \frac{T_u - T_y}{\tau_b} \tag{3b}$$

in which A_s is the area of steel reinforcement and T_y and T_u are the forces in the reinforcement corresponding to f_{sy} and f_{su}, respectively. It should be noted that τ_b, T_y, T_u and A_s are expressed per unit width throughout these formulations.

However, in a more heavily reinforced slab, or specimens containing relatively ductile steel, the concrete in the 'compressive ring' region may begin to crush before the reinforcement reaches f_{su}. The simplified analytical approach is adapted herein in order to predict the point at which this will occur. Towards this end, an equilibrium approach is adopted whereby concentrated compressive forces are considered at two contact points (A and C in Fig. 4). These are the locations most likely to crush as they experience the greatest concentration of compressive stress; this was also verified during the test programme (Cashell *et al.*, 2011). Considering Fig. 4 and applying moment equilibrium, the concentrated compression at the top fibre at points A and C (C_A and C_c, respectively) are found from:

$$C_A\left(\frac{L_1}{2}\right) = T_{sdy}\left(\frac{L_1}{2} - \frac{\eta L_1}{2}\right) + \frac{T_{sce}}{2}\left(\frac{L_1}{4} + \frac{\eta L_1}{2}\right) - T_{sdx}\left(\frac{L_2}{4}\right) - T_{scr}\left(\frac{L_2}{4}\right) \tag{4}$$

$$C_C = T_{scr} \tag{5}$$

where T_{sce}, T_{sdx}, T_{sdy} and T_{sce} represent the force in the steel reinforcement, per unit width, across the central yield line, diagonal yield line in the x-direction, diagonal yield line in the y-direction and the full-depth failure crack, respectively. A linear strain distribution is assumed between *A*-*B* and *C*-*B* as shown, whereby the strain at point *B* is a function of the reinforcement extension, in the appropriate direction, at this point. Meanwhile the concrete contraction at either *A* or *C*, in the limit, is assumed to be a function of the crushing strain for concrete, ε_{cr}, as shown in Fig. 4. From this, the distances X_A and Y_C are easily established.

The final assumption is that the maximum compressive stress-block depth is limited to 0.5*h* where *h* is the depth of the section. Accordingly, it is deduced that the concrete will crush at point *A* if:

$$\frac{2\left(T_{sdy} - C_A\right)}{hX_A} > f_c' \tag{6}$$

where f_c' is the concrete strength, whereas compression failure will occur at point *C* if:

$$\frac{2\left(C_C\right)}{hY_C} > f_c' \tag{7}$$

The solution procedure for this model is iterative, whereby an incremental load is applied to the member in sufficiently small steps until such a time as either the ultimate capacity of the steel reinforcement or the compressive capacity of the concrete, is reached. For every increment of load applied, the stress in the concrete is monitored at points *A* and *C* to ensure that it remains within the compressive capacity. Importantly, in addition to the overall response, the proposed method provides a means of finding the levels of deformation and load corresponding to failure, either by crushing of the concrete or fracture of the reinforcement. This represents a significant improvement on available analytical methods for assessing the ultimate response of reinforced concrete floor slabs. The reliability of the procedure will be investigated in a comparative assessment against the experimental results in subsequent sections.

4 Validation of slab models

In this investigation, the experimental results described in the companion paper (Cashell *et al*., 2011) are utilized to validate the proposed analytical models. In the first instance, attention is given to the overall load-deflection response using both the simplified analytical model (hereafter referred to as the SAM) and the finite element model (denoted as the FEM), and the most notable aspects of

the behaviour are highlighted. This is followed by a detailed analysis of the ultimate conditions, employing the SAM to assess failure. Further examination of the proposed failure assessment method is also provided by comparison against the results of another test series available in the literature (Bailey and Toh, 2007).

4.1 Load-displacement response

Table 1 gives a full comparison between experimental, analytical and numerical findings covering the key response parameters. To provide typical examples of the response, Figs. 5a and b present the experimental load-displacement together with the various analytical simulations for a number of tests that failed by reinforcement fracture (S-F60-M6-A) and concrete crushing (R-P120-D8-D), respectively. Similar comparisons have been carried out for all of the tests but these are not included herein for compactness.

The FEM analysis employs a mesh comprising 30×20 and 20×20 uniform-thickness shell elements for the rectangular and square specimens respectively, based on a mesh sensitivity assessment. On the other hand, it should be recalled that the SAM approach is based on rigid-plastic hardening behaviour and hence the elastic and elasto-plastic displacements are not captured. This procedure terminates upon either fracture of the reinforcement or crushing of the concrete and therefore the final point on each curve represents failure. The predictions provided by the SAM and FEM are further supplemented by the results of another analytical model which has been developed at the BRE (Bailey and Moore, 2000). This method assumes a similar crack pattern to the SAM and also ignores the elastic and elasto-plastic stages of the response.

The cracking load from each of the eighteen tests ($F_{cr,test}$), as well as the corresponding FEM prediction ($F_{cr,FEM}$), are given in Table 1. Evidently, the FEM provides a reasonable depiction of this point in most cases. Further evidence of this is provided in Fig. 5 as both the elastic response and the point of first cracking were closely matched by the FEM. In the post-yield range, the FEM predictions compares very favourably with the test data. However, there are some discrepancies in the results as multiple cracks occurred in the tests, particularly in the regions surrounding the load points, which is an effect that is not captured by the model.

The comparison plots show that the initial load resistance predicted by the SAM corresponds to values very close to the yield line capacity (F_u in Table 1). With an increase in displacement, the predicted behaviour provides a good representation of the experimental response in the plastic range. The prediction of maximum load capacity is almost identical to the actual behaviour, tending to be marginally conservative. Specimen S-F60-M6-A failed by rupture of the reinforcement

whereas failure of Specimen R-P120-D8-D (Fig. 5b) was governed by crushing of the concrete in the compressive-ring region. Also, it is noteworthy that ignoring the ribs of the profiled slab shape in the SAM analysis of R-P120-D8-D did not appear to have a significant effect on the load-deflection correlation. This is unsurprising given that the concrete only contributes to the load-carrying capacity in the post-cracking range through tension stiffening.

It is also evident that whilst the BRE prediction provides a reasonable correlation with the experimental response, the simplified analytical model generally has greater stiffness. This is expected as the SAM is based on an assumed kinematic mode whereas the BRE method is based on an assumed internal stress distribution. In addition, the SAM allows for an increase in the reinforcement force, whilst the BRE method assumes constant force corresponding to the yield strength of the steel with a constant increase of 10% along the through-depth crack. Furthermore, the favourable comparisons illustrated through these examples demonstrate the applicability of the kinematic expressions and the corresponding load-deflection response characteristics of the proposed analytical model.

The experimental and analytical studies discussed above provide valuable information pertaining to the ultimate behaviour of slabs. Further detailed assessment of the FEM results provides an insight into the predicted stress distributions and crack patterns over the slab. For example, Figs. 6 and 7 present more results from the finite element simulation of Tests S-F60-M6-A and R-P120-D8-D. Each figure depicts: (a) an overall view of the deformed slab at failure, (b) a magnified view of the deformed shape, indicating the stress distribution in the x-direction, and (c) a magnified image of the deformed shape including the distribution of stress in the transverse y-direction. Similar plots can be presented for all test specimens and can be found elsewhere (Cashell, 2009). The plots represent the behaviour at the failure deflection and the contours depict the stress on the top fibre of the concrete. Referring firstly to Fig. 6, considerable extension is evident in the central region of the slab, indicating the formation of a through-depth crack. Careful consideration of the stresses in the both directions identifies a compressive ring as well as classic yield lines and the through-depth crack. These are consistent with the experimental observations. Furthermore, the contours presented in Fig. 6 verify that the stress in the concrete remains within its compressive capacity before rupture of the reinforcement occurs. On the other hand, whilst Fig. 7 also clearly demonstrates yield line cracks and the compressive region, the concrete stress contours on the top surface (Figs. 7b and c) correctly predict that the crushing strength is surpassed in this case. As this is the top surface, the locations of highest stress in the concrete are around the central yield line crack and also the compressive ring region.

The favourable comparisons illustrated through these examples demonstrate the accuracy of the kinematic expressions and the corresponding load-deflection response characteristics of the proposed analytical model. In addition, the FEM simulations have been shown to capture the slab behaviour appropriately, with the stress distributions and crack formations comparing favourably with those observed in the tests.

4.2 Failure prediction

This section investigates the reliability of the simplified analytical model for predicting the point at which failure occurs, either by fracture of the reinforcement across a full depth crack or crushing of the concrete in the 'compressive-ring'. All of the eighteen slab tests described previously are used for calibration and validation. As shown before (Cashell, 2009; Cashell *et al*., 2010), within realistic limits, the bond strength has a relatively small effect on the load-deflection response whereas it has a pronounced influence on the failure level. It is therefore essential that a realistic representation of the idealised effective bond strength is employed for an accurate failure assessment. In this respect, the experimental data is effectively used to calibrate the value of τ_b. It is noteworthy that in the instances where compressive failure occurred, the experimental data can only be used to estimate an upper limit on the bond strength based on the assumption that a higher value would result in tension failure occurring prior to crushing.

The representative value of τ_b employed in the analysis of each slab is provided in Table 1. Also included in the table are the upper limits of the appropriate bond values for Tests R-F60-D8-A, R-F60-D8-C and R-P120-D8-D. The bond strength values reflect the bond force per unit length per unit width, and equate to approximately 10% of the equivalent bond stress values (in force per unit reinforcement cross-sectional area) for the specimens discussed in this paper. It is important to note that the SAM assumes that cracking only occurs along the yield lines as well as the through-depth failure crack. However, in reality, a much greater number of cracks developed in the tests, with the effect of relieving and redistributing the strain concentration in the steel, thereby delaying the attainment of ultimate strain and subsequent failure. Consequently, the value of τ_b utilised in the SAM implicitly incorporates this effect, and the relatively low values account for the formation of additional cracks.

It is also noteworthy that the bond strength assumed in the slab analysis is generally lower than the equivalent term employed in the one-way spanning strip analysis, as discussed elsewhere (Cashell *et al*., 2010). This is mainly owing to the two-way behaviour inherent to slabs, which distributes the strain in the steel in both directions and, most importantly, causes cracking to occur in two directions. Table 1 also includes the predictions for the failure deflection ($U_{f,SAM}$) and the

corresponding predicted failure load ($F_{f,SAM}$). Evidently, the results indicate that with a realistic assessment of the material and geometric properties, including those related to bond, a reasonable correlation is achieved between the analytical predictions and the test results.

As discussed previously, the predicted failure displacement is effectively calibrated using the experimental results, by adjusting the bond stress. Importantly, it is evident that the representative values of effective bond are similar for each bar-type, regardless of the other slab properties such as aspect ratio, depth, cross-section type or reinforcement ratio. In fact, the upper bond value of 0.04N/mm length per mm width could be applied to all slabs to yield a conservative prediction (noting that a value of 0.02N/mm length per mm width could also be more appropriately used for P6 bars). It is also noteworthy that the level of load corresponding to failure correlates particularly well with the test data.

As noted in the companion paper, the BRE analytical model includes an empirically-based equation to determine the deflection at failure, given by:

$$U_{f,BRE} = \sqrt{\left(\frac{0.5f_{sy}}{E_s}\right)_{reinforcement} \frac{3L_l^{\,2}}{8}} \tag{8}$$

where E_s is Young's modulus for the steel. Table 1 also includes the predicted failure displacements according to the BRE model ($U_{f,BRE}$) as obtained from Eq. (8). It is observed that the values predicted are typically over-conservative and do not account for several key geometric and material properties for each particular specimen. This approach adopts a simplified empirical approach, and ignores many of the salient parameters which have been shown to affect the ultimate conditions. Although a greater amount of information is required for the proposed SAM approach, it offers a more realistic approach for predicting the ultimate conditions.

4.3 Comparison against other results

It has been shown that the load-deflection response of floor slabs can be represented well using either a simplified analytical approach such as the SAM or BRE method, or alternatively, through a smeared-crack finite element procedure. However, the failure point is significantly more difficult to predict owing to the complexity of the mechanisms involved, and the large number of inter-related parameters which govern the behaviour. The robustness of the proposed SAM failure method is further assessed herein by examining selected results from another experimental investigation.

The tests conducted by Bailey and Toh (2007) are selected, and the experimental results are compared with analytical simulations. This programme included tests on simply-supported slabs which were subjected to uniform vertical loading, applied through an airbag. The geometric and material details of the specimens are summarised in Table 2 together with the analytical results. As before, the experimental failure displacement ($U_{f,test}$) is effectively used to calibrate the bond strength. To this end, a representative value for the effective bond strength (τ_b) has been determined to be in the order of 0.03-0.06N/mm length per mm width. These values inherently account for the degree of cracking that developed in each test. The table includes the predictions for the failure deflection ($U_{f,SAM}$) and the corresponding predicted failure load ($F_{f,SAM}$). The failure displacement predicted by the BRE analytical method (i.e. Eq. (8)) is also given in the table. Evidently, the results indicate that with a realistic representation of the material and geometric properties, a good correlation is achieved between the analytical predictions and the test results. Furthermore, although $U_{f,BRE}$ is rather conservative in most cases, it is un-conservative for both M9 and M10, both of which failed by concrete crushing. This highlights the importance of assessing failure based on the salient parameters influencing the ultimate conditions, such as the geometric configuration, bond characteristics, reinforcement ratio, and steel stress-strain response, amongst others.

5 Analytical assessment under elevated temperature

The preceding sections of this paper have provided a fundamental insight into the large-displacement response of reinforced concrete floor slabs with particular emphasis on ultimate behaviour and failure conditions. The focus has been on the ambient temperature behaviour as this represents an essential step towards a reliable assessment of the response at elevated temperature. In this section, the simplified analytical models described before are employed, together with finite element simulations, to investigate the ultimate behaviour of slab members under realistic fire conditions. The analytical approaches are calibrated and validated with reference to available experimental results. The information acquired in another experimental programme (Elghazouli *et al.*, 2009) is utilised within the various models in order to provide an accurate representation of the temperature-dependant material properties.

As expected, the behaviour of floor slabs in fire becomes relatively more complex than the ambient response as the strength, ductility and bond parameters are not only inter-related, but also non-linearly dependant on temperature. Furthermore, the elevated temperature response is dominated by thermal expansion and curvature effects, combined with the degradation of material strength. As a result, the flexural resistance reduces progressively with increasing temperature, although considerable load resistance can still be provided through the development of tensile catenary

action. In order to examine these issues further, both the ADAPTIC finite element model (FEM) and the simplified analytical approach (SAM) are utilised in this section. Both procedures are described and validated against available test results, where appropriate.

5.1 Finite element model (FEM)

The 2D shell element implemented in ADAPTIC and described previously (*cslb*) is also employed herein to simulate the slab response at elevated temperature. In addition to accounting for the geometric non-linearity due to large deformations, consideration is given to the response of concrete under a non-monotonic strain variation at elevated temperature (Izzuddin *et al*., 2004) In order to represent fire conditions, an initial gravity load is applied whilst a user-defined temperature distribution is applied through the cross-section and across the plan area of the member. For profiled slabs, the temperature distribution over both the trapezoidal and cover regions is accounted for, as shown in Fig. 8, where θ_i and $\Delta\theta_i$ indicate respectively temperatures and temperature increments between the bottom of the cover and the top of the slab.

The material models previously described in earlier sections of this paper are employed again in this analysis, with due consideration given to the effect of elevated temperature on key characteristics. To this end, the material properties are assumed to follow independent tri-linear relationships with varying elevated temperature (Fig. 9). Each slab is represented using a mesh comprising 30×20 shell elements, based on a mesh sensitivity assessment. The temperature-dependant material properties $E_{s,\theta}$, $f_{sy,\theta}$, $f_{su,\theta}$ $\varepsilon_{su,\theta}$ and $f_c{}',_\theta$ are summarised in Table 3; piecewise linear interpolation is used for temperatures between the values indicated in the table. The effect of temperature on the strength and stiffness parameters is presented as a reduction factor, i.e. a proportion of the respective value at ambient temperature. Similarly, the ultimate strain of the steel at varying levels of elevated temperature ($\varepsilon_{su,\theta}$) is represented using a tri-linear enhancement curve using the values given in the table. The steel characteristics were determined from more detailed studies into the effect of elevated temperature on reinforcement properties (Elghazouli *et al*., 2009). On the other hand, the concrete parameters were represented using a trilinear idealisation based on information obtained from available sources (Morley and Royles, 1983; EN 1992-1-2, 2004). The coefficient of thermal expansion for steel (α_s) is considered as 14×10^{-6}.

5.2 FEM Simulations

A number of researchers have conducted elevated temperature slab tests in recent years (Lim *et al*., 2002; Foster *et al*., 2004; Bailey and Toh, 2007). These investigations have primarily focussed on representing the overall deformation response and load-carrying capacity with increasing

temperature, without giving detailed attention to the factors which influence the limiting conditions. Notwithstanding that, the results are employed herein to validate the overall response predicted by the ADAPTIC (FEM) slab model. On the other hand, failure is examined in the subsequent section, using the SAM. It noteworthy that, in certain cases, published studies only include basic material properties of the test specimens; hence some assumptions have to be made and these are discussed where appropriate. The experimental measurements have been approximately digitized from printed graphical curves.

Each of the elevated temperature slab tests which are examined herein comprised specimens with various geometric and material parameters which were free to move both laterally and rotationally at the supports. Heating was introduced at a constant rate of 5°C/min by Bailey and Toh (2007) until a maximum temperature of 1000°C was reached. On the other hand, Lim *et al.* (2002) applied the ISO 834 (1999) standard fire for a duration of 3 hours, while Foster *et al.* (2004) did not provide information on the approach used for temperature application. All slabs examined by Bailey and Toh as well as Foster *et al.* failed by fracture of the reinforcement through a full-depth failure crack, which developed across the short span. On the other hand, none of the slabs examined by Lim *et al.* were reported to have failed when the tests were terminated after 3 hours. It is worth noting that only the specimens tested by Lim *et al.* were of realistic dimensions compared with actual slabs.

Analytical comparisons are carried out hereafter for slabs from each test series, for which experimental results are available. For brevity, a selection of specimens is chosen from each test series for analysis, and these are representative of the range of parameters examined within each programme. The results provided hereafter are typical of the comparisons for all tests. The details of the specimens are summarised in Table 4, which gives the details corresponding to the long and short span (L_1 and L_2), depth (h), reinforcement ratio (ρ), concrete strength (f_c') and steel yield strength (f_{sy}). All slabs had a flat cross-section. Also included in the table, where information is available, are temperature measured at the top surface (θ_t), at the level of the reinforcement (θ_s) and also at the bottom surface (θ_b) at the end of each test, as well as the levels of load ($F_{f,test,\theta}$) and displacement ($U_{f,test,\theta}$) which were sustained at this point. The total imposed load during each test is F_{imp}. This was applied either through dead weights (Bailey and Toh, 2007) a hydraulic jack (Foster *et al*, 2004) or by using large water drums (Lim *et al*, 2002). As before, the material properties are related to temperature in the analysis using trilinear degradation curves according to the information presented previously (Morley and Royles, 1983; EN 1992-1-2, 2004; Elghazouli *et al*., 2009).

The comparative deformation-temperature histories for the above-described tests are illustrated in Fig. 10a-c. The correlation between the numerical predictions and the available experimental data is

very good in all cases and a reasonable approximation is obtained for the level of deflection at a given temperature. Some discrepancies exist and may be attributed to modelling idealisations (e.g. the use of a bi-linear steel model), or the variability of assumed material characteristics. It should be noted that in the FEM analysis, an initial displacement is depicted at ambient temperature due to the applied gravity loading. This is not included in the presented test data of Lim *et al*. and is not represented in the corresponding figure (Fig. 10c). Nevertheless, it can be seen that the slabs in each test program deformed at a similar rate at the beginning of heating and accelerated as the failure point was approached. The tests of Bailey and Toh, and also Foster *et al.*, all of which failed by reinforcement rupture, reached a maximum temperature of between 550-750°C. The tests by Bailey and Toh had a relatively large span/depth ratio and therefore demonstrated greater deflection. It should be noted that the numerical prediction of the test by Lim *et al*. does not capture accurately the initial pattern of rapid deflection driven by thermal gradient effects. This may be attributed to modelling idealisation including simplified representation of the temperature distribution within the slab

The FEM simulations were also used to gain a more detailed insight into the ultimate slab behaviour. For example, Figs. 11a and b show the predicted concrete stress distributions on the top surface for slab MF1 from the experiments of Bailey and Toh. It is evident that the maximum predicted compressive stress in the concrete is around 8N/mm^2. At ambient temperature, the compressive strength of the concrete was 43.2N/mm^2 which, in accordance with the information described in EN 1992-1-2 (2004) reduces by around 70% to 13N/mm^2 at 750°C. Therefore, the model correctly predicts that concrete crushing does not occur prior to rupture of the reinforcement.

The results in this section clearly demonstrate the overall reliability of the finite element model in predicting the large displacement response of floor slabs under elevated temperatures. It provides a useful insight into the underlying behavioural mechanisms which influence the response. In the following section, the elevated temperature simplified failure assessment approach is validated against available test results.

5.3 Simplified analytical model (SAM)

The purpose of the elevated temperature simplified analytical model is to: (i) provide a depiction of the full load deflection history under steady-state temperature application; and (ii) predict the level of load and displacement corresponding to failure at a particular temperature. The focus in this section is given to validating the second of these points, using available experimental data from the test programme of Bailey and Toh (2007).

The slab SAM accounts for the influence of thermal expansion and curvature in addition to the deterioration in material properties. In this section, the slabs considered are simply-supported and therefore it is assumed that they are free to expand in any direction as well as free to curve in the direction perpendicular to the slab edges. Moreover, the strips parallel to the edges are allowed to curve freely at the interior end of the slab whilst decreasing to zero curvature at the supports. Also, the triangular and trapezoidal parts of the slab are assumed to expand and curve independently. The extent of curvature of a strip across the slab is determined by the thermal gradient and thermal properties of the concrete, which are user-defined. Based on the strip analysis, it is assumed that the temperature distribution is uniform over the slab plan and varies linearly through the cross-section. Accordingly, the chord length of each strip element within the slab (L_c) elongates due to thermal expansion whilst shortening owing to thermal curvature according to Omer *et al*. (2006):

$$L_c = L + \alpha_c \Delta\theta_s L - \frac{\kappa^2 L^3}{24} \tag{9}$$

where L is the ambient strip length and κ is the thermal curvature assuming a linear thermal gradient through the cross-section.

Failure is defined as the point where the reinforcement fractures across the full-depth crack and the steel stress reaches its ultimate strength. However, since the reinforcement stretches across both the full-depth crack and the diagonal yield line in the x-direction, the assessment of the failure deflection ($U_{f,SAM,\theta}$) is not straightforward. Therefore, a simplified approach has been developed whereby the force in the steel across each crack is assumed to be represented by the force in the steel at the centre of each of the regions (i.e. central yield line crack, diagonal yield line crack and the full depth crack across the short span). The force in the reinforcement ($T_{s,\theta}$) is given by Omer *et al*. (2006):

$$T_{s,\theta} = T_{y,\theta} + \sqrt{A_s E_{2,\theta} \tau_{b,\theta} \left[\Delta_s - \left(\alpha_s - \alpha_c \right) \Delta\theta_s L/2 \right]} \tag{10}$$

where $T_{y,\theta}$ and $\tau_{b,\theta}$ are the yield force in the reinforcement and the bond strength, respectively, at elevated temperature. Finally, the failure deflection ($U_{f,SAM,\theta}$) is determined as the maximum of U_{f1} and U_{f2}, with U_{f1} obtained from Omer *et al*. (2006):

$$U_{f1} = \sqrt{d_s^2 - \kappa\eta^2 L_1^2 d_s - \frac{\kappa^2 \eta L_1^4 \left(1-2\eta\right)^2}{24} + \frac{\eta L_1 \left(T_{u,\theta} - T_{y,\theta}\right)^2}{A_s E_{2,\theta} \tau_{b,\theta}}} - d_s \tag{11}$$

where d_s is the effective depth to the reinforcement, and U_{f2} is determined from Eq. (12):

$$U_{f2} = \sqrt{\frac{\left(T_{u,\theta}-T_{y,\theta}\right)^2 L_1}{2A_s E_{2,\theta}\tau_{b,\theta}} - \frac{\kappa^2 L_1^4 \left(1-2\eta\right)^3}{384}} \qquad \text{if} \quad \frac{T_{u,\theta}-T_{y,\theta}}{\tau_{b,\theta}} < \frac{L_1}{4}\left(1-2\eta\right)$$

(12)

$$U_{f2} = \sqrt{\frac{\left(T_{u,\theta}-T_{y,\theta}\right)L_1^2\left(1-2\eta\right)}{4A_s E_{2,\theta}} - \frac{\kappa^2 L_1^4\left(1-2\eta\right)^3}{384} - \frac{\tau_{b,\theta}L_1^3\left(1-2\eta\right)^2}{32A_s E_{2,\theta}}} \quad \ldots \quad \text{if}$$

$$\frac{T_{u,\theta}-T_{y,\theta}}{\tau_b} > \frac{L_1}{4}\left(1-2\eta\right)$$

5.4 Failure assessment at elevated temperature

Although several researchers have conducted experiments on floor slabs at elevated temperature, as discussed before, only Bailey and Toh (2007) have published information relating to failure of the specimens. Consequently, this study compares these experimental results with analytical predictions from the SAM. As before, the material properties at elevated temperature are assumed to follow the trends to those presented in Table 3, and discussed in detail elsewhere (Elghazouli *et al*., 2009) The calculated failure deflections ($U_{f,SAM,\theta}$) and corresponding loads ($F_{f,SAM,\theta}$) are given in Table 5 for each test, together with the actual test values for failure deflection and load ($U_{f,test,\theta}$ and $F_{f,test,\theta}$, respectively) and the temperature measured at the level of the reinforcing mesh at failure (θ_s). The representative effective bond values employed in the models ($\tau_{b,\theta}$) are calibrated using the experimental failure displacement values. Limited information is available on the actual test behaviour such as crack patterns and, therefore, the ambient bond strength employed in the analysis was maintained at a constant value of 0.03N/mm per mm width for all of the tests. This value degraded with elevated temperature, according to the information available (Sager and Rostasy, 1982) to between 0.005-0.007N/mm per mm width, depending on the temperature range. It should be recalled that the model assumes that cracks only form in the locations predicted by yield line theory as well as the through-depth failure crack and hence, the bond strength employed in the model implicitly accounts for any additional cracks that develop. This test programme also included similar tests at ambient temperature, as discussed earlier in this paper. These contained identical reinforcement and the corresponding bond strength was found to be around 0.03-0.06N/mm per mm width. These values are similar to those established for the ambient slab tests discussed in the companion paper. This implies that, within the temperature range of 550°C-750°C, the bond strength drops to about 10-20% of its ambient value.

Since the emphasis in this section is on the ultimate behaviour, further examination of the failure conditions is carried out by modifying the bond strength used in the previous analysis, whilst retaining each of the other parameters. Slabs MF1 and MF7 are selected for illustrative purposes as these specimens represent a range of failure temperatures. The curves in Fig. 12 depict the enhanced failure displacement that is obtained for relatively low bond strength values, because of the reduced strain concentrations. Although MF1 exhibited relatively higher levels of deflection than MF7 owing to greater thermal expansion effects, similar trends were generally observed in both cases.

6 Conclusions

This paper described models which were developed to assess the ultimate response of floor slabs with various material and geometric configurations. Two analytical approaches have been proposed: (i) a simplified analytical model (SAM) which is based on fundamental principles; and (ii) an advanced nonlinear numerical method, referred to as the FEM, which is implemented in ADAPTIC. Both account for the tensile catenary stage of the behaviour which develops when the specimen has undergone large levels of deflection. In addition to the overall response, the SAM also quantifies the limiting criteria of the specimen, considering that failure is governed either by rupture of the reinforcement across a full-depth crack or crushing of the concrete within the compressive ring.

The validity of the analytical procedures was examined by comparison against the experimental results described in the companion paper. Importantly, this also includes a fundamental failure-prediction assessment, thereby overcoming a significant shortcoming of previously developed empirical approaches. Previous slab models do not deal with this issue adequately, and the failure is based on semi-empirical average strain considerations thus providing results that are independent of the bond and other reinforcement characteristics. The model was first developed by Omer *et al*. (2006, 2010) for slabs with and without planar restraint, and focussed on the behaviour of lightly reinforced slabs. Hence, it was assumed that failure was by fracture of the reinforcement across a through-depth failure crack. However, this was extended in this paper to consider the possibility that failure can occur due to crushing of concrete in compression.

This paper has discussed the effect of reinforcement ratio, bar-type, span-to-depth ratio, aspect ratio and cross-section type on the ultimate performance of slab members. The agreement between the numerical simulations and experimental findings demonstrated the overall reliability of the analytical models in predicting the large displacement response of floor slabs. Furthermore, it was shown that with an appropriate representation of the material and geometric properties, a close prediction of both the failure deflection and corresponding load can be obtained.

The ambient study was also extended to a more focussed assessment of the elevated temperature response. Under these conditions, structural members such as floor slabs can be subjected to very high temperatures, which influence the response through the degradation of the material properties in addition to the effects of thermal expansion and curvature. These effects have been accounted for in the numerical procedures, which were then compared to available experimental data and favourable correlations were obtained. It was established that the temperature of the steel reinforcement, and the consequent effect on its strength and ductility, is the most significant factor on the behaviour. Overall, it was demonstrated that the proposed analytical approaches capture the main behavioural mechanisms which determine the behaviour in fire. Furthermore, they provide a realistic and efficient evaluation of the limiting conditions.

The findings presented in this paper, together with the simplified expressions proposed in the companion paper, provide the necessary tools for the development of performance-based failure criteria required within a framework for the fire design of composite steel concrete floor slabs. Further research is nonetheless necessary into certain aspects of the behaviour, especially those related to the bond-slip characteristics under elevated temperatures. However, the studies presented herein represent a significant step towards replacement of the current prescriptive approaches which unrealistically disregard key parameters influencing slab failure under fire conditions.

7 Acknowledgements

The funding provided by the UK Engineering and Physical Sciences Research Council (EPSRC) under Grant No EP/C511204 for the work described in this paper is gratefully acknowledged.

8 References

Bailey C.G. and Toh W.S. (2007). "Small-scale concrete slab tests at ambient and elevated temperatures." *Engineering Structures*, **25**:2775-2791.

Bailey, C.G. and Moore, D.B. (2000). "The structural behaviour of steel frames with composite floor slabs subject to fire. Part 2: Design." *The Structural Engineer*, **78**(11):28–33.

Cashell K.A., Elghazouli A.Y. and Izzuddin B.A. (2011). "Failure assessment of lightly reinforced slabs – Part I Experimental assessment". Accepted for publication in the *Journal of Structural Engineering*. (companion paper).

Cashell, K.A. (2009). "Failure assessment of floor slab systems under extreme loading conditions." *PhD Thesis*, Imperial College London.

Cashell, K.A., Elghazouli, A.Y. and Izzuddin B.A. (2010). "Experimental and analytical assessment of ductility in lightly reinforced concrete members." *Engineering Structures*, **32**(9): 2729-2743.

Clifton, G.C. (2006). “Design of Composite Steel Floor Systems for Severe Fires.” Report R4-131, New Zealand Heavy Engineering Research Association.

Elghazouli A.Y., Cashell K.A. and Izzuddin B.A. (2009). “Experimental evaluation of the mechanical properties of steel reinforcement at elevated temperature.” *Fire Safety Journal*, 44(6):909-919.

Elghazouli, A. Y. and Izzuddin, B. A. (2001). “Analytical assessment of the structural performance of composite floors subject to compartment fires.” *Fire Safety Journal*, **36**: 769–793.

Elghazouli, A.Y. and Izzuddin, B.A. (2004). “Realistic modelling of composite and reinforced concrete floor slabs under extreme loading. II: Verification and application.” *Journal of Structural Engineering*, ASCE **130**(12):1985–1996.

EN 1992 Eurocode 2 (2004). “Design of concrete structures: Part 1.2: General rules – Structural fire design.” *European Committee for Standardization*, Brussels.

Foster S.J., Burgess I.W. and Plank R. (2004). “High-temperature experiments on model-scale concrete slabs at high displacements.” *Third International Workshop for Structures in Fire,* Ottawa, Canada.

ISO 834 (1999). “Fire resistance tests - elements of building construction.” *International Organization for Standardization*, Geneva, Switzerland.

Izzuddin, B.A. (1994). “Nonlinear dynamic analysis of framed structures.” *PhD Thesis*, Imperial College, University of London.

Izzuddin, B.A. and Elghazouli, A.Y. (2004). “Failure of lightly reinforced concrete members under fire. I: Analytical modelling.” *Journal of Structural Engineering*, **130**(1):3–17.

Izzuddin, B.A., Moore, D.B. (2002). “Lessons from a Full-Scale Fire Test.” *Structures and Buildings*, Proceedings of the Institution of Civil Engineers, **152**(4):319-329.

Izzuddin, B.A., Tao, X.Y. and Elghazouli, A.Y. (2004). “Realistic modelling of composite and reinforced concrete floor slabs under extreme loading. I: Analytical method.” *Journal of Structural Engineering*, ASCE **130**(12):1972–1984.

Lim, L., Buchanan, A. and Moss, P. (2002). “Experimental testing and numerical modelling of two-way concrete slabs under fire conditions.” *Journal of the Structural Engineering Society New Zealand*, SESOC, 12-26.

Morley P.D. and Royles R. (1983). “Response of the bond in reinforced concrete to high temperatures.” *Magazine of Concrete Research,* **35**(123):67-74

Omer, E., Izzuddin B.A. and Elghazouli A.Y. (2010). “Failure of unrestrained lightly reinforced concrete slabs under fire, Part I: Analytical models.” *Engineering Structures*, 32(9): 2631-2646.

Omer, E., Izzuddin, B.A., Elghazouli, A.Y. (2006). “Failure assessment of simply supported floor slabs under elevated temperature.” *Structural Engineering International*, **16**:148 – 155.

Sager, H. and Rostasy, F.S. (1982). “The effect of elevated temperature on the bond behavior of embedded reinforcing bars.” *Bond in Concrete*, P. Bartos, ed., Applied Science Publishers, London, 206-216.

9 Tables

Table 1 Experimental results

Test	Bar Type	Failure Mode	F_u (kN)	$F_{f,test}$ (kN)	$U_{f,test}$ (mm)	$F_{cr,test}$ (kN)	$F_{cr,FEM}$ (kN)	$\frac{F_{cr,test}}{F_{cr,FEM}}$	τ_b (N/mm/mm)	$F_{f,SAM}$ (kN)	$\frac{F_{f,test}}{F_{f,SAM}}$	$U_{f,SAM}$ (mm)	$\frac{U_{f,test}}{U_{f,SAM}}$	$U_{f,BRE}$ (mm)	$\frac{U_{f,test}}{U_{f,BRE}}$
R-F60-M6-A	M6	tension	46.3	71.7	69	31.1	26.1	1.19	0.025	67.7	1.06	67	1.03	50	1.37
R-F60-P6-A	P6	punching	20.9	61.5	126	27.8	25.4	1.09	0.020	48.2	1.28	120	1.05	34	3.71
S-F60-M6-A	M6	tension	48.6	82.2	64	34.1	31.7	1.08	0.023	77.1	1.07	63	1.03	33	1.93
R-F40-D6-B	D6	tension	32.3	56.6	90	9.8	11.2	0.88	0.026	56.4	1.00	89	1.01	51	1.75
R-F60-D6-C	D6	tension	48.4	104.5	84	23.1	22.4	1.03	0.040	88.5	1.18	83	1.01	51	1.63
R-F60-D6-A	D6	tension	40.4	72.5	76	20.6	20.0	1.03	0.038	75.5	0.96	75	1.01	51	1.48
S-F60-D6-A	D6	tension	51.3	87.6	68	23.2	20.1	1.15	0.027	87.2	1.00	67	1.02	34	2.00
S-F60-D6-D	D6	tension	108.8	167.5	63	25.8	23.2	1.11	0.030	167.8	1.00	63	1.00	34	1.83
S-F60-D8-D	D8	tension	106.0	179.5	64	28.2	26.4	1.07	0.033	170.2	1.05	64	1.00	33	1.93
S-F60-P6-A	P6	punching	22.1	64.0	98	33.3	31.5	1.06	0.020	42.6	1.50	90	1.08	22	4.44
R-F60-M6-A	M6	tension	46.3	78.3	74	24.4	24.2	1.01	0.025	78.3	1.00	72	1.02	50	1.48
R-F40-M6-B	M6	tension	30.7	57.6	83	11.1	10.8	1.03	0.026	56.9	1.01	82	1.01	50	1.66
R-F60-D8-A	D8	compression	53.5	91.9	83	26.1	25.5	1.02	< 0.1	94.7	0.97	80	1.03	50	1.65
R-F60-D8-C	D8	compression	65.8	123.1	88	24.2	24.7	0.98	< 0.1	120.0	1.03	70	1.25	50	1.75
R-P120-M6-A	M6	tension	46.3	73.5	51	50.1	57.2	0.88	0.031	68.6	1.07	51	1.00	50	1.02
S-P120-M6-A	M6	tension	48.6	89.0	50	52.2	51.5	1.01	0.026	78.7	1.13	50	1.00	33	1.51
R-P120-D8-D	D8	compression	93.6	141.8	75	37.3	38.2	0.98	< 0.2	141.2	1.00	72	1.03	50	1.49
S-P120-D8-D	D8	tension	94.6	178.5	58	63.7	66.6	0.96	0.035	180.7	0.99	57	1.02	33	1.75

Table 2 Details and analysis of tests by Bailey and Toh [13]

Test	L_1 (mm)	L_2 (mm)	h (mm)	d (mm)	ρ	f_{sy} (N/mm^2)	f_{su} (N/mm^2)	f_c' (N/mm^2)	$F_{f,test}$ (kN)	$U_{f,test}$ (mm)	τ_b (N/mm/mm)	$F_{f,SAM}$ (kN)	$\frac{F_{f,test}}{F_{f,SAM}}$	$U_{f,SAM}$ (mm)	$\frac{U_{f,test}}{U_{f,BRE}}$	$U_{f,BRE}$ (mm)	$\frac{U_{f,test}}{U_{f,BRE}}$
M1	1700	1100	18.2	2.42	0.198	732	756	41.3	38.8	73	0.03	45.2	0.86	71	1.02	43	1.67
M2	1100	1100	19.1	2.42	0.198	732	756	38.0	32.7	60	< 0.1	38.5	0.85	60	1.01	28	2.15
M3	1700	1100	22.0	1.53	0.079	451	487	35.3	23.0	85	0.06	28.4	0.81	84	1.02	34	2.50
M4	1100	1100	20.1	1.53	0.090	451	487	35.3	22.1	65	0.06	24.6	0.90	64	1.01	22	2.95
M5	1700	1100	189.9	1.47	0.174	406	500	27.9	33.5	68	< 0.2	36.5	0.92	68	1.00	32	2.10
M6	1100	1100	21.6	1.47	0.140	406	500	38.6	32.7	48	< 0.2	37.1	0.88	47	1.03	21	2.29
M7	1700	1100	20.4	0.84	0.061	599	653	41.6	16.2	50	0.04	18.5	0.87	49	1.02	39	1.26
M8	1100	1100	19.0	0.84	0.065	599	653	42.9	12.9	30	0.04	16.4	0.79	29	1.01	25	1.17
M9	1700	1100	22.0	0.66	0.052	450	470	37.6	13.7	22	0.06	14.5	0.95	21	1.03	34	0.65
M10	1100	1100	19.7	0.66	0.061	450	470	37.3	12.0	20	0.06	13.5	0.89	19	1.02	22	0.89
M11	1700	1100	18.6	2.42	0.313	732	756	39.8	16.6	72	< 0.05	18.2	0.91	70	1.04	43	1.67
M12	1100	1100	19.4	2.42	0.274	732	756	40.7	19.6	65	< 0.05	20.8	0.94	64	1.01	28	2.33
M13	1700	1100	36.6	2.42	0.082	732	756	42.0	54.5	54	0.03	56.9	0.96	53	1.02	43	1.25
M14	1100	1100	35.9	2.42	0.088	732	756	40.2	49.8	46	0.03	52.0	0.96	45	1.01	28	1.64

Table 3 Variation of material properties with temperature

	Reduction/enhancement factors		
Temperature Range (°C)	20-100	100-300	300-700
$E_{s,\theta}/E_s$	1	0.79	0.12
Temperature Range (°C)	20-100	100-300	300-700
$f_{sy,\theta}/f_{sy}$	1	0.76	0.26
Temperature Range (°C)	20-300	300-500	500-700
$f_{su,\theta}/f_{su}$	1	0.51	0.2
Temperature Range (°C)	20-100	100-300	300-700
$\varepsilon_{su,\theta}/\varepsilon_{su}$	1	1.12	2.33
Temperature Range (°C)	20-200	200-600	600-1200
$f_c'_{,\theta}/f_c'$	1	0.6	0

Table 4 Details of elevated temperature tests

Reference	Slab	L_1 (mm)	L_2 (mm)	h (mm)	ρ (%)	f_c' (N/mm^2)	f_{sy} (N/mm^2)	θ_t (°C)	θ_s (°C)	θ_b (°C)	F_{imp} (kN)	$F_{f,test,\theta}$ (kN)	$U_{f,test,\theta}$ (mm)
Bailey and Toh, 2007 [16]	**MF1**	1700	1100	19.7	0.159	43.2	695	672	765	840	9.87	5.28	181
	MF2	1700	1100	23.1	0.129	43.3	684	604	747	826	10.32	5.52	140
	MF9	1700	1100	21.6	0.042	47.1	371	553	652	723	6.92	3.70	152
Foster *et al.*, 2004 [23]	**2**	850	550	14.0	0.150	37.0	260	200	510	700	1.38	1.38	-
	3	850	550	14.0	0.150	37.0	260	200	510	700	2.15	2.15	-
	4	850	550	15.0	0.150	37.0	260	200	510	700	2.18	2.18	-
Lim et *al.*, 2002 [4]	**661**	4150	3150	100.0	0.295	36.6	568	250	700	1100	39.22	70.59	210
	D147	4150	3150	100.0	0.198	36.7	565	250	700	1100	39.22	70.59	270
	HD12	4150	3150	100.0	0.565	36.6	468	300	750	1050	39.22	70.59	150

Table 5 Predicted failure displacements for Bailey and Toh tests [16]

Slab	$U_{f,test,\theta}$ (mm)	$U_{f,SAM,\theta}$ (mm)	$\frac{U_{f,test,\theta}}{U_{f,SAM,\theta}}$	$F_{f,test,\theta}$ (kN)	$F_{f,SAM,\theta}$ (kN)	$\frac{F_{f,test,\theta}}{F_{f,SAM,\theta}}$	θ_s (°C)
MF1	181	180	1.01	5.28	5.17	1.02	765
MF2	140	133	1.05	5.52	5.41	1.02	747
MF3	131	128	1.02	3.66	3.38	1.08	727
MF4	124	118	1.05	5.43	5.11	1.06	700
MF5	137	125	1.10	5.28	5.02	1.05	722
MF6	144	140	1.03	7.89	7.59	1.04	782
MF7	94	90	1.04	4.46	4.19	1.07	557
MF8	100	97	1.03	4.65	4.47	1.04	654
MF9	152	145	1.05	3.70	3.57	1.04	652
MF10	104	101	1.03	5.49	5.46	1.01	686

10 Figures

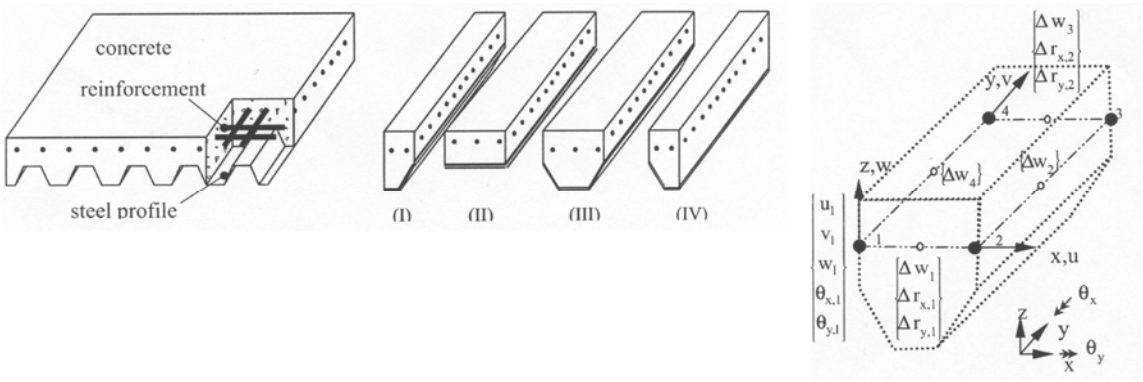

Figure 1 Composite slab element developed in ADAPTIC [5]

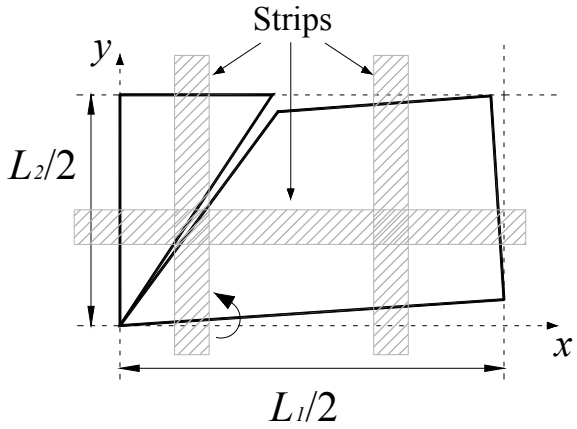

Figure 2 Schematic representation of the deformed shape slab configuration

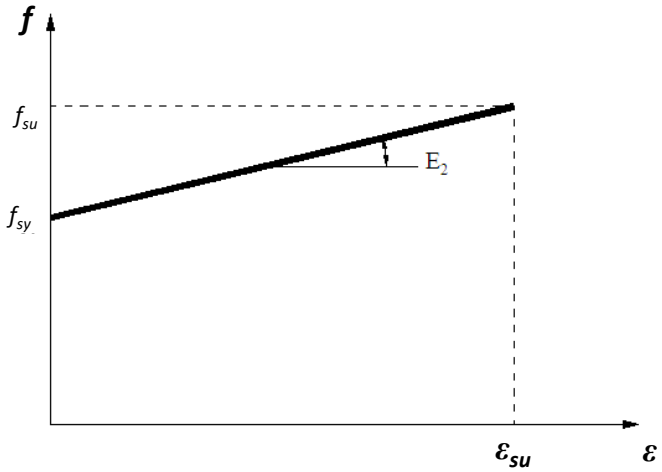

Figure 3 Steel material model in simplified analytical model

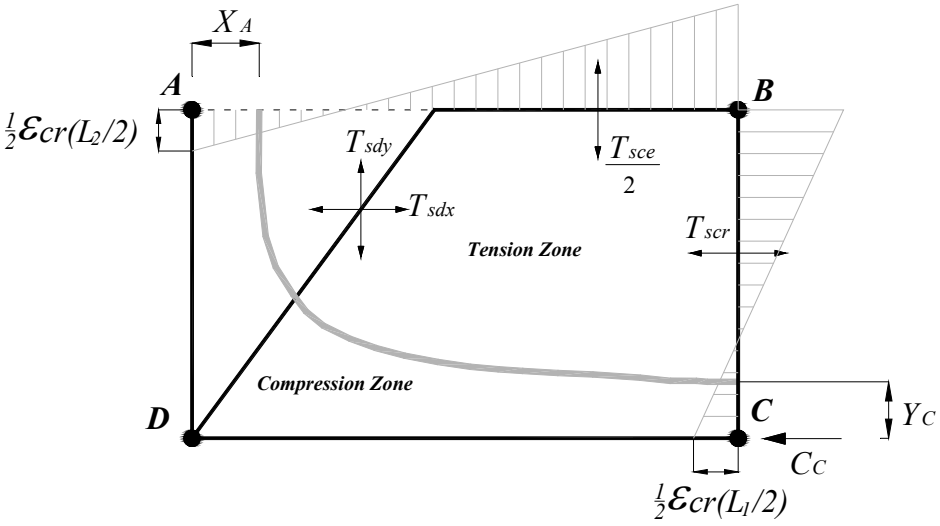

Figure 4 Stress distribution for concentrated concrete compression

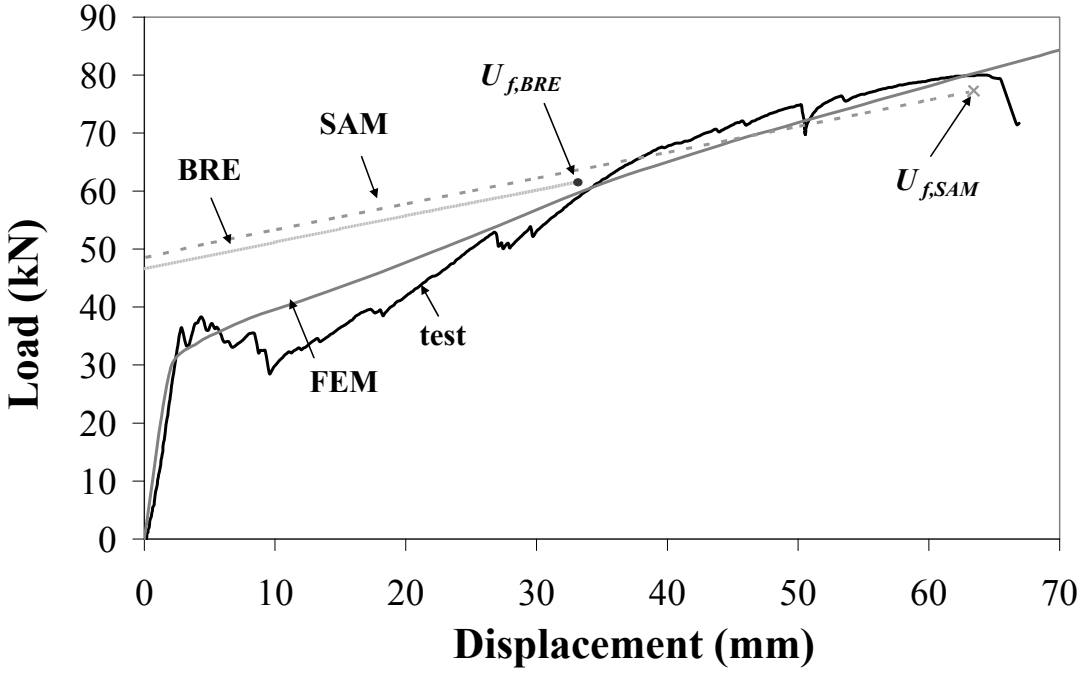

(a) S-F60-M6-A

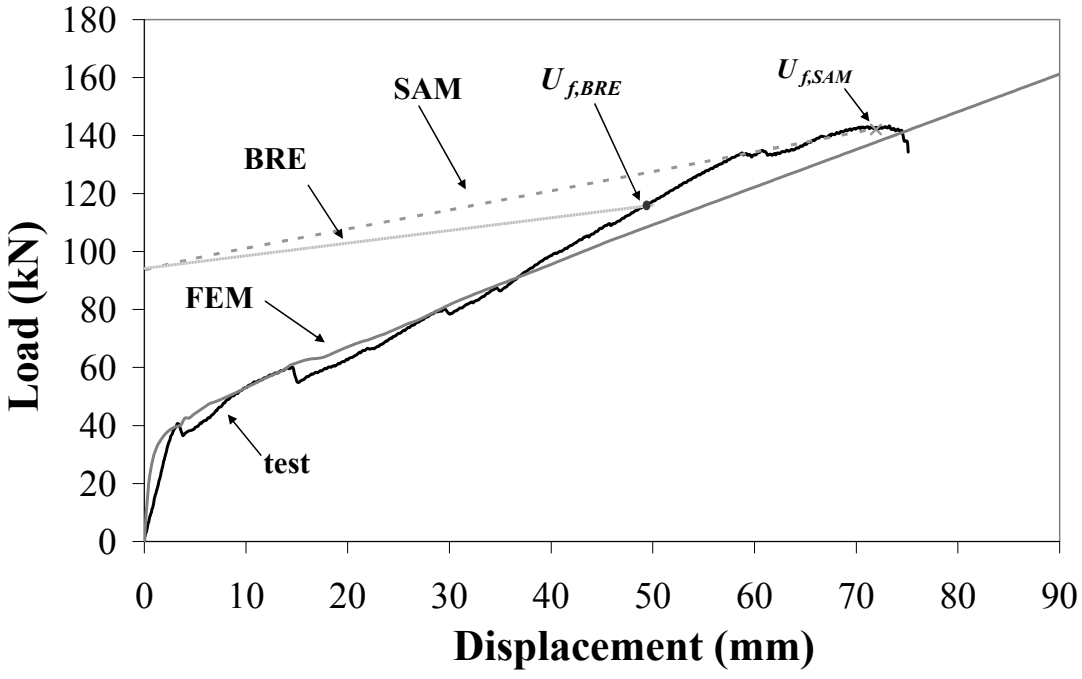

(b) R- P120-D8-D

Figure 5 Load-Deflection comparison plots

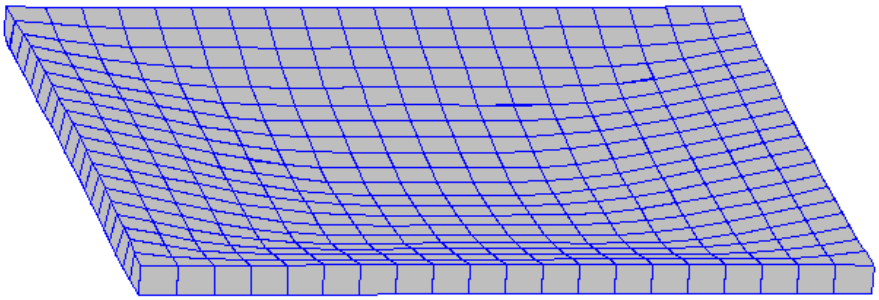

(a) deflected shape (deformation scale 1:1)

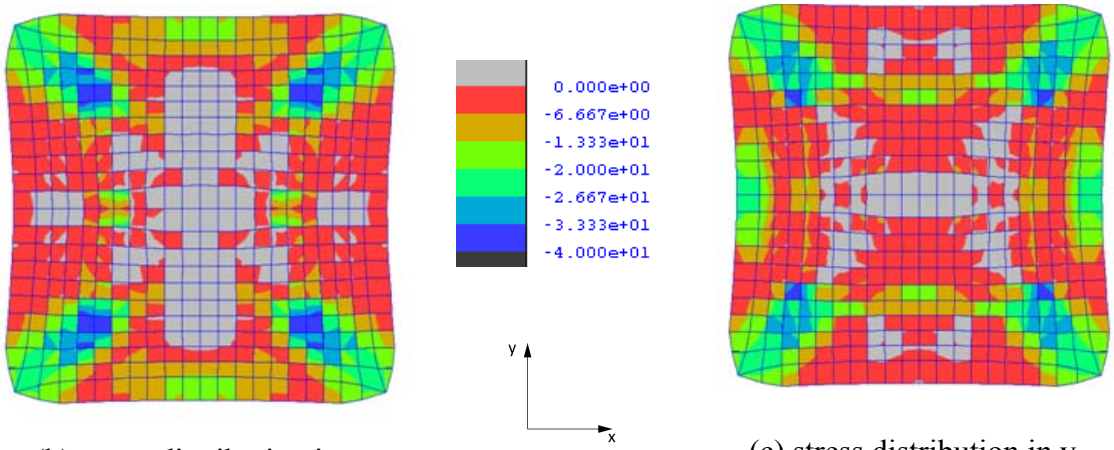

(b) stress distribution in x-direction (deformation scale 10:1)

(c) stress distribution in y-direction (deformation scale 10:1)

Figure 6 FEM analysis of S-F60-M6-A

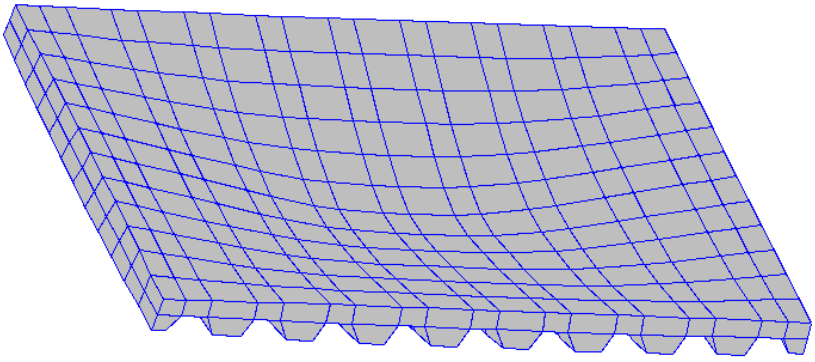

(a) deflected shape (deformation scale 1:1)

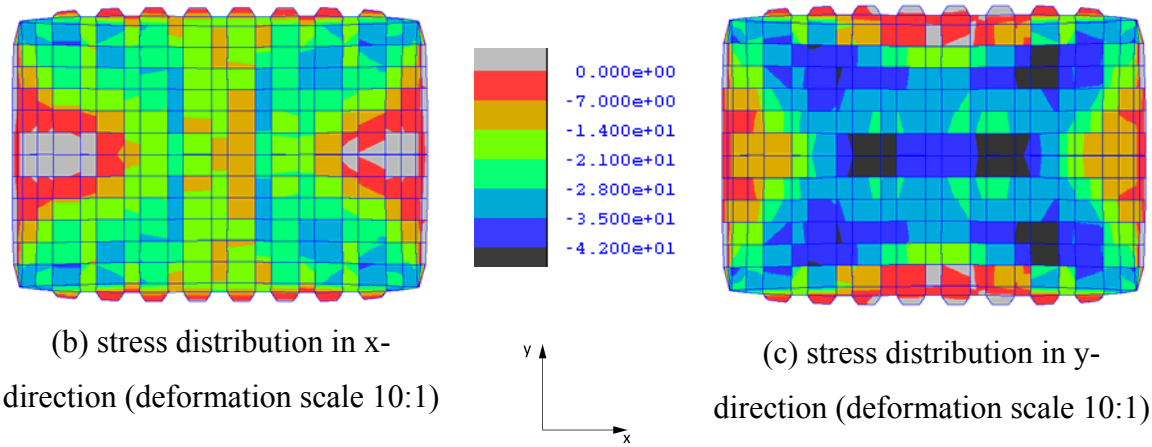

(b) stress distribution in x-direction (deformation scale 10:1)

(c) stress distribution in y-direction (deformation scale 10:1)

Figure 7 FEM analysis of R-P120-D8-D

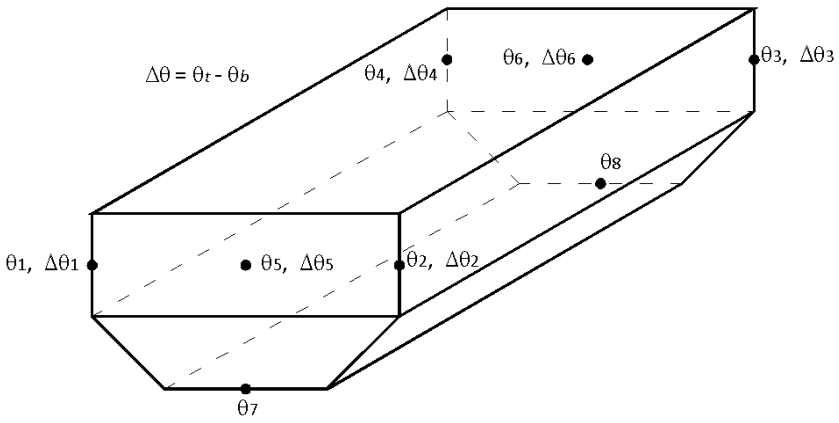

Figure 8 Slab temperature input

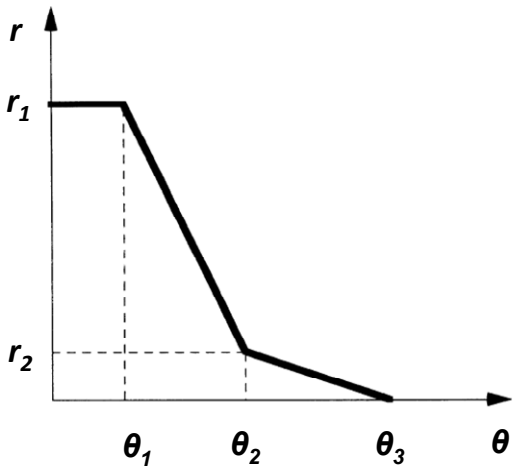

Figure 9 Variation of material reduction factors with temperature

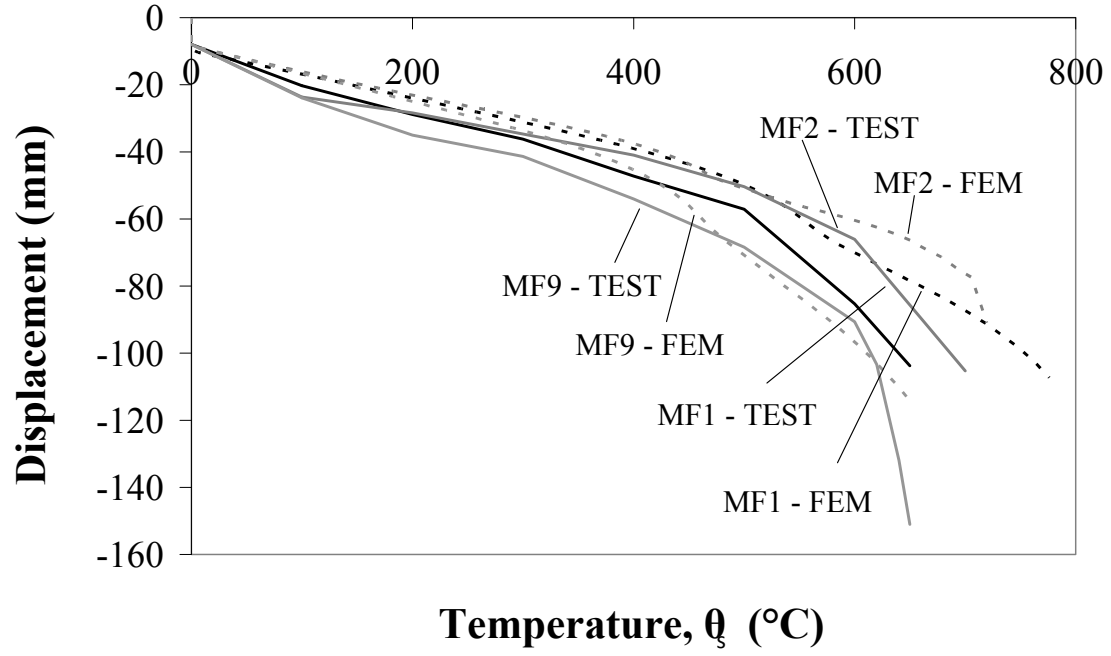

(a) Bailey and Toh [15]

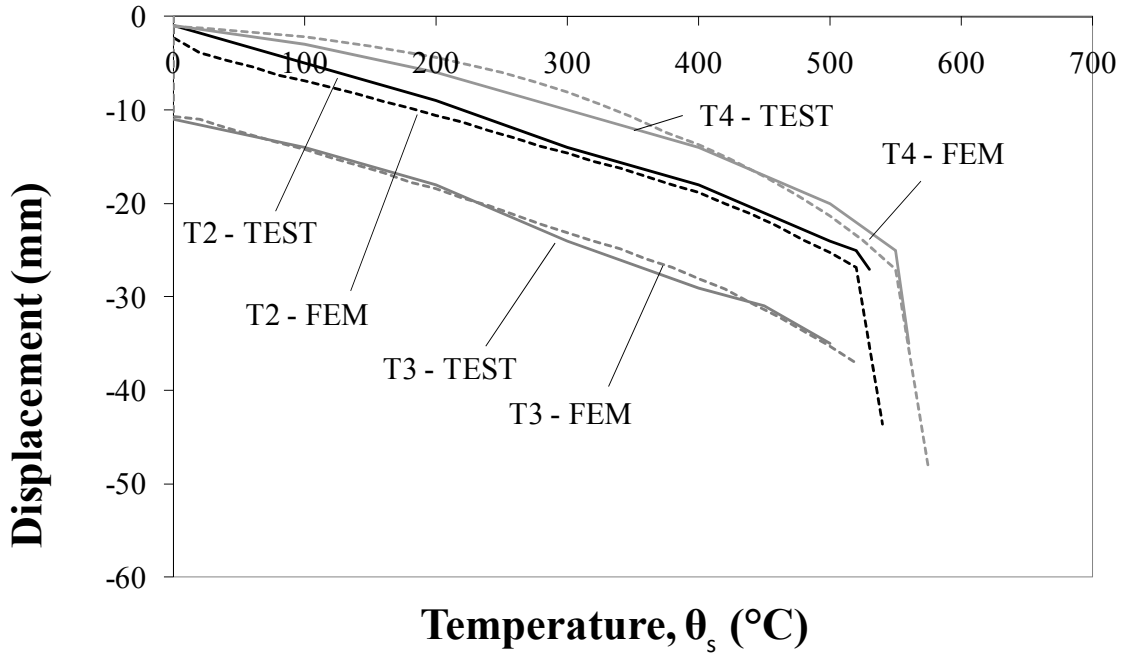

(b) Foster et al. [19]

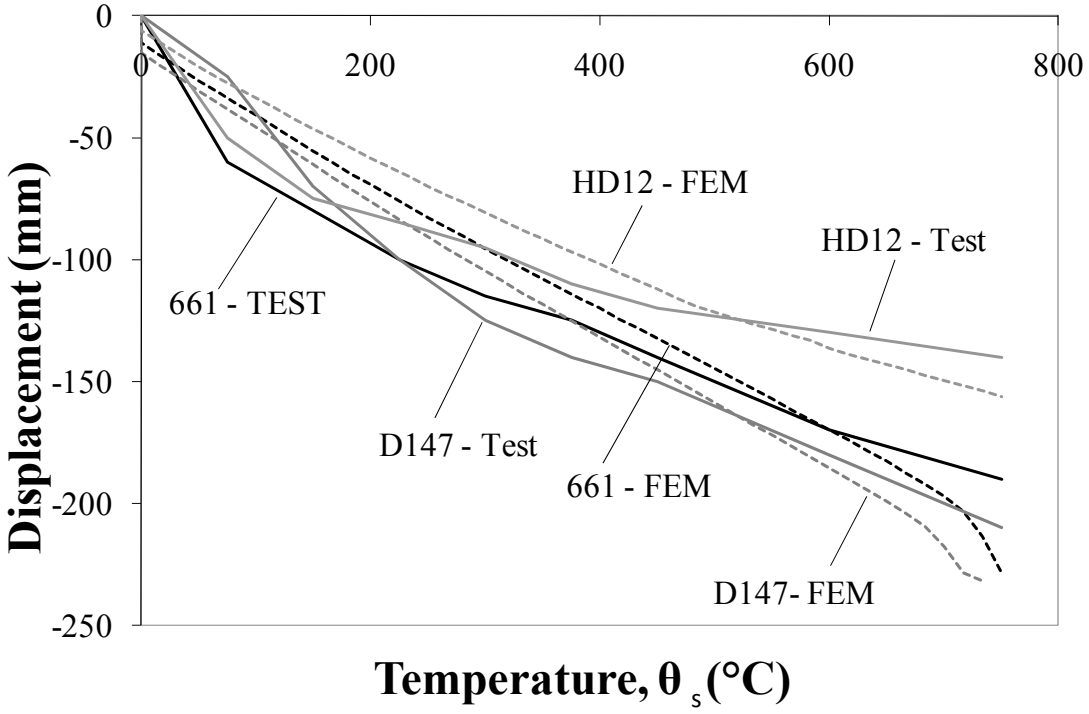

(c) Lim *et al.* [3]

Figure 10 ADAPTIC predictions of elevated temperature slab experiments (contd.)

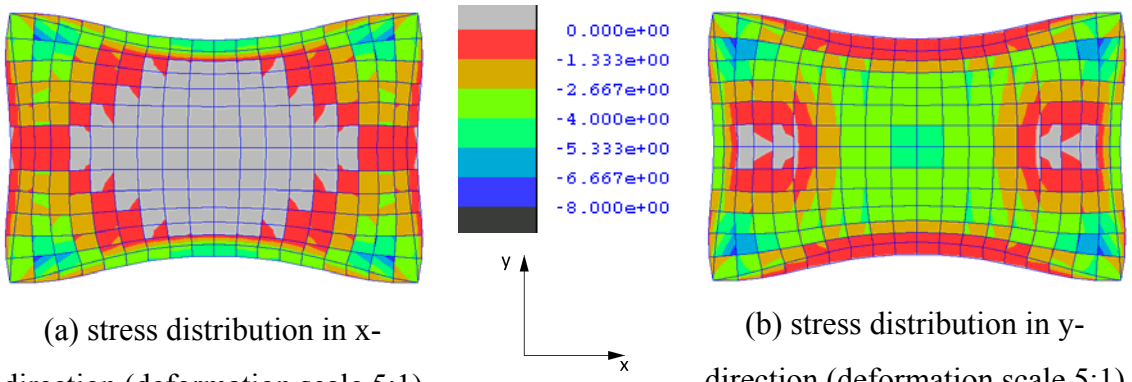

(a) stress distribution in x-direction (deformation scale 5:1)

(b) stress distribution in y-direction (deformation scale 5:1)

Figure 11 FEM simulation of concrete stress distributions for MF1

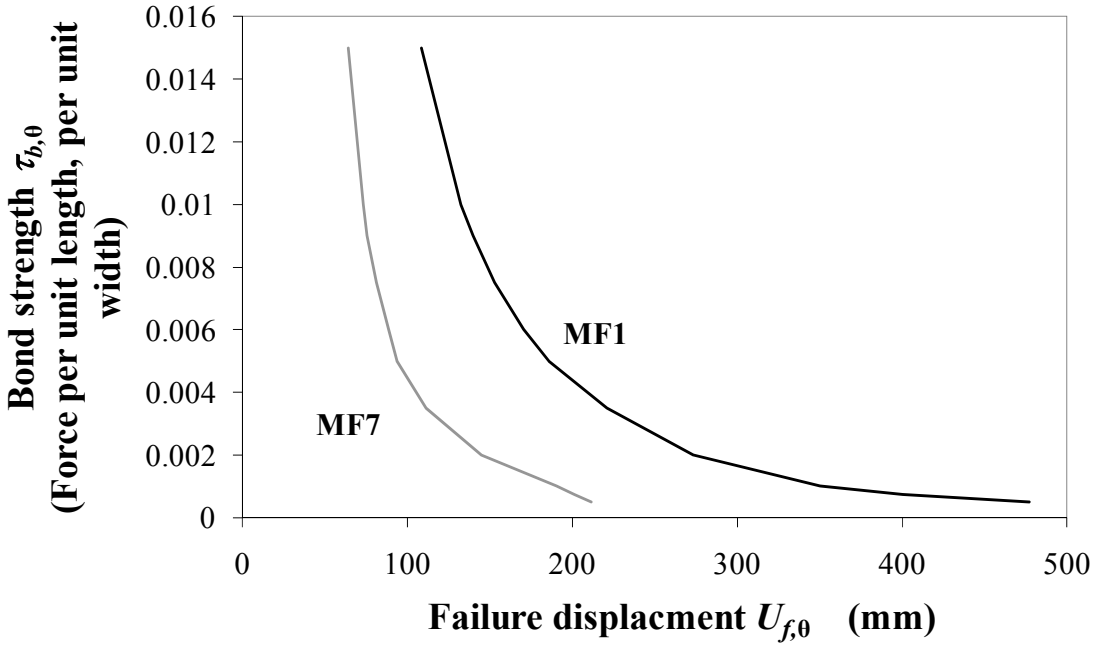

Figure 12 Influence of bond strength on failure displacement for MF1 and MF7